

A Novel Technique for Smearing Links

Robert W. Johnson

Fusion Research Center, Georgia Institute of Technology, Atlanta, GA 30332, USA^{*}

(Dated: November 14, 2006)

Abstract

Traditional smearing or blocking techniques serve well to increase the overlap of operators onto physical states but allow for link directions only along lattice axes. Recent attempts to construct more general propagators have shown promise at resolving the higher spin states but still rely on iterative smearing. A new construction is here presented which creates smeared links from (sparse) matrix multiplications, allowing propagation at arbitrary directions. As an application and example, we compute the positive-parity, even-spin glueball spectrum up to spin 6 for pure gauge SU(2) at $\beta = 6$ in D=2+1.

PACS numbers: 11.15.Ha, 12.38.Lg, 12.39.Mk

^{*}Electronic address: rob.johnson@gatech.edu; URL: http://www.frc.gatech.edu/Rob_Johnson.htm

I. INTRODUCTION

Operator construction in lattice gauge theory relies on the use of smeared and/or blocked links to improve the overlap onto physical states. (See [1] for a review of $SU(N)$ gauge theory in 2+1 dimensions.) Smearing serves to reduce the ultraviolet fluctuations, allowing for a better projection onto the physically smooth wave-functions of glueball (and other) states, and blocking serves to keep the operator size physical as the lattice spacing decreases. Unfortunately, traditionally smeared links are only defined along axes directions, allowing construction of at most 4-fold symmetric operators, with the rotation symmetries of the cubic lattice. These operators couple to states with spin $|J|$ congruent *modulo* 4, *ie* a trial spin 0 operator may contain contributions from spins 0, 4, 8, *etc*, and a trial spin 1 operator may contain contributions from spins 1, 3, 5, *etc* [2, 3]. To remedy the situation, links along either arbitrary or diagonal directions have been constructed [2, 4], allowing for operators with higher-order symmetry. These have been successful at resolving the 0/4 and 1/3 ambiguities [5, 6] in the 2+1 dimensional pure gauge theory spectrum.

The “path constructor method” of [4] creates a blocked link along the diagonal lattice directions for each blocking level, which is used in a projection algorithm to define a link between arbitrary sites i and j in a given timeslice. While effective, care must be taken of the details of the path construction for each unique arrangement of i and j . The “matrix method” of [2, 4] creates the matrix of Green’s functions between any and all sites i and j from the inversion of a matrix formed from the link variables of the timeslice, with a “hopping parameter” included to control the effective smearing level. While a single algorithm constructs all the paths at once, the inversion is painfully slow compared to iterative blocking and care must be taken to suppress unwanted torelon contributions. Note, however, that the correlation of rotated segment operators shown in [4] is much smoother for the matrix method, implying a better approximation of rotational invariance. Further, the matrix method appears to be directly applicable to fermion propagator calculations with some minor modification [4, 7, 8]. For these reasons, further investigation of the matrix method is warranted.

In this article, we explore a new method of smeared link construction based upon the matrix method but which alleviates its primary difficulties. Matrix inversion is replaced with matrix multiplications and torelons need not be suppressed as they are not constructed. Pre-

liminary results for SU(2) in D=2+1 at $\beta=6$ are promising. Section II reviews the technique of constructing operators of arbitrary spin J . Section III describes how to construct smeared “superlinks” between arbitrary sites using matrix multiplications. In Subsection IV A we construct “traditional” operators for Polyakov loops and for spins 0 and 2 glueball operators. Construction of 8-fold operators is demonstrated in Subsection IV B, and “clock” operators with 12-fold symmetry are in Subsection IV C. Section V presents results on an $L=16$ lattice. Some considerations and suggested improvements follow in Section VI, and we conclude by summarizing.

II. CONSTRUCTION OF OPERATORS WITH ARBITRARY SPIN ON A CUBIC LATTICE

To resolve the *modulo* 4 ambiguity in spin of conventional operators, one needs to construct operators of arbitrary spin from gauge-invariant loops at relative angles $2\pi/n$ other than the $\pi/2$ commonly available on the cubic lattice. These operators will suffer from their own *modulo* n spin ambiguities determined by the n -fold symmetry employed, but knowledge is power, and control over the value of n lets one select which sector of the spectrum one resolves. Loops which are π -symmetric will resolve the positive-parity, even-spin sector, and loops which are not π -symmetric will be able to resolve the full spectrum.

Consider a timeslice of D=2+1 in the continuum. Let \mathcal{C} be the trace of the gauge field along an arbitrarily shaped closed loop of contour C aligned to the axes. Copies rotated through an angle θ are denoted \mathcal{C}_θ . Then, to construct a gauge invariant operator \mathcal{O}_J of arbitrary spin J , we take the weighted average over all loops \mathcal{C}_θ , where the weight is the complex phase $e^{iJ\theta}$:

$$\mathcal{O}_J = \frac{1}{2\pi} \oint d\theta e^{iJ\theta} \mathcal{C}_\theta . \quad (1)$$

On the lattice timeslice, our choice of angles is restricted to the n -fold angles of our chosen operator

$$\mathcal{O}_J \rightarrow \frac{1}{2\pi} \sum_{j=1}^n \Delta\theta_j e^{iJ\theta_j} \mathcal{C}_{\theta_j} , \quad (2)$$

and our loops \mathcal{C}_{θ_j} will no longer be exact rotational copies of each other. Following [3], we normalize all the loops relative to their root-mean-square vacuum expectation value, so that

they each have equivalent vevs, *ie*

$$\mathcal{C}_{\theta_j} \rightarrow \mathcal{C}_{\theta_j} \times \sqrt{\langle\langle \mathcal{O}_{\theta_j}^2 \rangle\rangle_j / \langle\langle \mathcal{O}_{\theta_j}^2 \rangle\rangle}, \quad (3)$$

where $\langle\cdots\rangle_j$ denotes the average over angles j . Vacuum-subtracted correlation functions are defined by

$$C_J(t) = \langle \mathcal{O}_J^\dagger(t) | \mathcal{O}_J(0) \rangle - \langle \mathcal{O}_J^\dagger \rangle \langle \mathcal{O}_J \rangle, \quad (4)$$

which will be normalized to $C_J(0) = 1$. For complex-valued operators we take the real part of Equation (4) as our correlation function. Similarly, we can compute the normalized cross-correlation for states of different J :

$$C_{\tilde{J}J}(t) = \frac{\langle \tilde{\mathcal{O}}_{\tilde{J}}^\dagger(t) | \tilde{\mathcal{O}}_J(0) \rangle}{\sqrt{\langle \tilde{\mathcal{O}}_{\tilde{J}}^\dagger | \tilde{\mathcal{O}}_{\tilde{J}} \rangle \langle \tilde{\mathcal{O}}_J^\dagger | \tilde{\mathcal{O}}_J \rangle}}, \quad (5)$$

where the tilde over \mathcal{O} implies the vacuum-subtracted operator. Taking $t = 0$ in Equation 5 gives us the timeslice overlap between the operators. To save computational time, we restrict ourselves in this article to using loops which are π -symmetric. If we formed closed loops that were not symmetric under a rotation by π , we could recover both even and odd spins and both positive and negative parity, otherwise phase cancellations restrict us to the positive-parity, even-spin sector.

III. SMEARED LINKS FROM MATRIX MULTIPLICATION

To construct our arbitrarily shaped loops, we need to evaluate smeared links between arbitrary sites in the timeslice. We start by defining a matrix \mathcal{M} of dimension $L^{D-1} \times L^{D-1}$ whose elements, themselves $SU(N)$ matrices (giving a total matrix dimension of $NL^{D-1} \times NL^{D-1}$), are constructed from the timeslice links $U_{i,j}$ from sites i to sites j as follows:

$$\mathcal{M}_{i,j} = \begin{cases} 0 & \text{if sites } i \text{ and } j \text{ are not nearest neighbors} \\ U_{i,j} & \text{if sites } i \text{ and } j \text{ are nearest neighbors} \end{cases}. \quad (6)$$

Previously [2, 4], Green's functions were calculated by noting that

$$\mathcal{K} \equiv \frac{1}{1 - \alpha \mathcal{M}} \approx 1 + \alpha \mathcal{M} + \alpha^2 \mathcal{M}^2 + \dots \quad (7)$$

for some small parameter α which behaves much like a “hopping parameter” for the gauge field. The matrix \mathcal{M}^k consists of all paths of length k —for even L , the odd powers of \mathcal{M}

are traceless while the even powers of \mathcal{M} have a trace consisting of all paths of length k which terminate at their starting site, including those which double back on themselves. The diagonal elements of \mathcal{M}^2 are “unity paths”, 4 for each site, *ie* $Tr\mathcal{M}^2/4NL^{D-1} = 1$. The expectation value of the spatial plaquette $\langle U_{\square}^S \rangle$ may thus be written as

$$\langle U_{\square}^{M^4} \rangle \equiv (Tr\mathcal{M}^4/NL^{D-1} - 28)/8 . \quad (8)$$

Note that this formula corrects that given previously [4, 9], as there are actually 7 paths which contribute unity per lattice direction and each plaquette is counted 8 times (4 corners by 2 orientations).

Rather than compute the inverse matrix \mathcal{K} , which suffers from torelon contributions coming from the terms in the infinite series with $k > L/2$, we compute the sequence of matrices \mathcal{M}^k for $k \in \{1, k_{max}\}$. For $k_{max} > L/2$ torelon contamination is determined by the locations of sites i and j —we may propagate up to a total distance of L along a pure diagonal before contamination sets in. In practice we take $k_{max} = L$ to allow maximum propagation and avoid contamination by judicious choice of superlink orientation when constructing operators, or we may simply remove operators *ab initio* which appear to have been contaminated. Note that our parameter α has disappeared—we may reintroduce a smearing level parameter by applying a number p of smearing iterations before constructing our matrices \mathcal{M}^k (pre-smearing level p). We may now use our superlinks $\mathcal{M}_{i,j}^{k,p}$ to construct our gauge-invariant loops.

In order to reduce the count of unity paths contributing to our \mathcal{M}^k , first we form

$$\widetilde{\mathcal{M}}^2 = \mathcal{M}^2 - diag(\mathcal{M}^2) , \quad (9)$$

where we have removed the diagonal elements of \mathcal{M}^2 . Then we construct our sequence of matrices iteratively:

$$\widetilde{\mathcal{M}}^{2k+1} = \widetilde{\mathcal{M}}^{2k} \times \mathcal{M} , \quad (10)$$

$$\widetilde{\mathcal{M}}^{2k+2} = \widetilde{\mathcal{M}}^{2k} \times \widetilde{\mathcal{M}}^2 - diag(\widetilde{\mathcal{M}}^{2k} \times \widetilde{\mathcal{M}}^2) , \quad (11)$$

removing the diagonals of the even powers as we go. As these matrices are sparse, performing the multiplications may be executed quite efficiently, and storage requirements are modest—the superlink construction requires a fraction of the memory needed to compute the cross-correlations of the binned operators. We may verify our construction by checking that the

spatial plaquette equals

$$\langle U_{\square}^{\widetilde{\mathcal{M}}^4} \rangle \equiv (Tr \widetilde{\mathcal{M}}^4 / NL^{D-1} - 12) / 8 , \quad (12)$$

indicating a reduction in unity paths from 28 to 12. If we examine the superlinks along axes directions, we see that to propagate a distance l between sites i and j along an axis, one should take $\widetilde{\mathcal{M}}_{i,j}^{l+2}$, and to propagate a distance l off-axis we use $\widetilde{\mathcal{M}}_{i,j}^l$, where l is defined to be the number of links in the shortest path between sites i and j .

IV. CONSTRUCTION OF POSITIVE-PARITY OPERATORS

A. Construction of Traditional Operators

Operators for Polyakov loops may be constructed in D-1 directions, at sizes l for which L/l is an integer, simply by taking the product of superlinks along an axis $\hat{\mu}$

$$\mathcal{O}_{P, \hat{\mu}}^l = \prod_{m=0}^{L/l-1} \widetilde{\mathcal{M}}_{i+ml\hat{\mu}, i+(m+1)l\hat{\mu}}^{l+2} , \quad (13)$$

see Figure 1. “Box” operators of size l centered at site i may be formed as

$$\mathcal{O}_{\square}^l = \widetilde{\mathcal{M}}_{i+l\hat{\mu}, i+l\hat{\nu}}^l \times \widetilde{\mathcal{M}}_{i+l\hat{\nu}, i-l\hat{\mu}}^l \times \widetilde{\mathcal{M}}_{i-l\hat{\mu}, i-l\hat{\nu}}^l \times \widetilde{\mathcal{M}}_{i-l\hat{\nu}, i+l\hat{\mu}}^l , \quad (14)$$

where $\hat{\mu}, \hat{\nu}$ are orthogonal directions, Figure 2. “Bar” operators, longer along the $\hat{\mu}$ axis than the $\hat{\nu}$, may be built using the clock points defined below as

$$\begin{aligned} \mathcal{O}_{B, \hat{\mu}}^l = & \widetilde{\mathcal{M}}_{X4_l, Xm1_l} \times \widetilde{\mathcal{M}}_{Xm1_l, X2_l} \times \widetilde{\mathcal{M}}_{X2_l, X10_l} \\ & \times \widetilde{\mathcal{M}}_{X10_l, Xm2_l} \times \widetilde{\mathcal{M}}_{Xm2_l, X8_l} \times \widetilde{\mathcal{M}}_{X8_l, X4_l} , \end{aligned} \quad (15)$$

where $Xm1_l$ is the on-axis midpoint between $X2_l$ and $X4_l$, $Xm2_l$ is between $X2_l$ and $X4_l$, and similarly for $\mathcal{O}_{B, \hat{\nu}}^l$; see Figure 3. Operators of spin 0 and 2 are constructed from the bar operators as the normalized sum and difference of $\mathcal{O}_{B, \hat{\mu}}^l$ and $\mathcal{O}_{B, \hat{\nu}}^l$, *ie*

$$\mathcal{O}_{n, J}^l = \mathcal{O}_{4, 0/2}^l = (\mathcal{O}_{B, \hat{\mu}}^l \pm \mathcal{O}_{B, \hat{\nu}}^l) / \sqrt{2} . \quad (16)$$

Note that these operators are π -symmetric 4-fold operators, hence the subscript 4. States with spins $|J|$ congruent *modulo* 4 will have equivalent phases and hence the greatest mutual

overlap, *ie* spins 0/4, 2/6, and 1/3 if we were using traditional L-shaped loops, will be mixed. The state with the lowest spin might not be the lightest state in a channel, thus care must be taken when assigning spin quantum numbers to the calculated states. The gaps between the 0⁺ and 4⁺ and between the 2⁺ and 6⁺ are assumed to be large enough that the lower spin dominates the lightest few states.

B. Construction of 8-fold Operators

To achieve a degree of symmetry greater than the traditional 4-fold operators, we develop an algorithm to select points in a timeslice which are at relative angles of approximately $2\pi/8$ by placing an octagon on the lattice and labeling the points at size l as A_l through H_l clockwise; see Figure 4. Using these we may construct 8-fold π -symmetric bar operators, *eg*

$$\mathcal{O}_8^l = \widetilde{\mathcal{M}}_{B_l, A_l}^d \times \widetilde{\mathcal{M}}_{A_l, F_l}^d \times \widetilde{\mathcal{M}}_{F_l, E_l}^d \times \widetilde{\mathcal{M}}_{E_l, B_l}^d, \quad (17)$$

with $d = d(l)$ chosen appropriately, Figure 5, allowing us to resolve the spin 0/4 ambiguity. In practice, midpoints are also defined (as for the bar operators of the previous subsection) so that contamination is avoided. To build operators $\mathcal{O}_{8,J}^l$ with even spin J , we take the weighted linear combinations as above, Equation (2). States with spins $|J|$ congruent *modulo* 8 will have equivalent phases and hence the greatest mutual overlap, *ie* spins 0/8, 2/6, and 4/12 will be mixed, but the overlap between the spin 0 and spin 4 should be minimal.

C. Construction of Clock Operators

As before, we develop an algorithm to select points in a timeslice which are at relative angles of approximately $2\pi/12$; in other words, we place an imaginary clock face on the lattice centered at site X with increasing sizes and select those sites closest to where the hour marks would be, hence the appellation “clock” to operators made from this set of points. See Figure 6. We label these points at size l as 1_l through 12_l , clockwise naturally.

We define 6 rhomboid shaped loops at angles $\theta_j = j\pi/6$ for $j \in \{0, \dots, 5\}$, *eg*

$$\mathcal{O}_\diamond^l = \widetilde{\mathcal{M}}_{X, 8_l}^d \times \widetilde{\mathcal{M}}_{8_l, 6_l}^d \times \widetilde{\mathcal{M}}_{6_l, 4_l}^d \times \widetilde{\mathcal{M}}_{4_l, X}^d, \quad (18)$$

see Figure 7. To build operators $\mathcal{O}_{12,J}^l$ with even spin J , we take the weighted linear combinations as above. States with spins $|J|$ congruent *modulo* 12 will have equivalent phases

and hence the greatest mutual overlap, *ie* spins 0/12, 2/10, 4/8, and 6/18 will be mixed.

V. RESULTS

A. Calculation Details

To evaluate the performance of our smearing technique, we calculate the above operators for pure gauge SU(2) on an $L=16$ lattice at $\beta=6$ with 30,000 measurements taken every 10 compound sweeps, both with ($p=1$) and without ($p=0$) pre-smearing. Thermal updates are done via the Kennedy-Pendleton heat bath algorithm [10] augmented with a 4:1 ratio of over-relaxation sweeps [11] and global gauge transformations every 19 sweeps. After selecting a set of operators based on their auto-correlation functions, cross-correlations are computed and used in a variational procedure to extract the lightest few states in each channel [1]. Timeslice overlaps are computed to check the spin decomposition of the final states.

Zero-momentum states are constructed by averaging operators over the timeslice. Effective masses are extracted from the normalized correlation functions for $t \geq 1$ via the formula

$$m_{\text{eff}}^J(t) = \log \left(\frac{C_J(t-1)}{C_J(t)} \right). \quad (19)$$

In principle one should include a term representing correlations the other way around the periodic lattice, but in practice such effects are swamped by the statistical noise, especially for the heavier states. Errors are calculated using the jackknife procedure [7].

B. Calculated Spectra

In Table I we compare the vacuum expectation values for the lattice plaquette and spatial plaquette computed directly and the spatial plaquette computed via \mathcal{M}^4 and $\widetilde{\mathcal{M}}^4$. Our directly computed plaquettes are well within errors of the accepted value [1], and our superlink plaquettes agree perfectly with the direct spatial plaquette. Table II displays the effective masses for the Polyakov loops after applying the variational procedure. Interestingly, the size 4 Polyakov loop operators produced no signal (and were removed from the calculation) even though they should have had no torelon contamination—perhaps an intrinsic fluctuation of the Polyakov loop precludes coupling to the size 4 loop operator. The 0^+ box

operator's masses are shown in Table III, and the 0^+ and 2^+ bar operators' masses are in Table IV. These masses compare well with the values given by Teper. The 0^+ , 2^+ , and 4^+ masses for the 8-fold operators are shown in Table V. These 8-fold operators returned a very noisy signal for the 4^+ which showed evidence of vacuum contamination (as evidenced by a nonzero vev for the correlation function), and so an explicit vacuum subtraction was incorporated. Even so, the 8-fold 4^+ operators failed to return a robust signal, and the timeslice overlaps (shown in Table VI) clearly display significant overlap with the 0^+ operators. The third operator displays the only plateau, and while its overlap (30%) with the 0^+ channel is not the least, its mass is chosen as our 8-fold estimate. Tables VII and VIII display the spectrum for the 0^+ , 2^+ , 4^+ , and 6^+ 12-fold operators. Again the 4^+ correlation functions exhibited vacuum contamination, but at a much reduced level compared to the 8-fold operator, and explicit vacuum subtraction seemed not to help. Looking at the timeslice overlaps in Tables IX and X, a significant *mod* 4 overlap still exists, and masses for the higher spins 4 and 6 should be taken as provisional at this stage. (Overlaps between the 0/4 and 2/6 channels are generally less than 1%.) For the 12-fold 4^+ , the third operator is chosen despite its 48% overlap with the 0^+ channel as its mass compares well with previous estimates, and for the 6^+ the eighth operator is chosen as it is the only one to display a plateau in the effective mass. The best estimates for the mass plateau values are highlighted in boldface in the tables. Masses are in lattice units, and jackknife errors on the last few digits are shown in parentheses following the mass. Zeros represent effective masses which were negative or imaginary as the correlation functions descended into noise.

With 30,000 measurements taken, one would have expected cleaner signals from the various operators. The displayed statistical errors for the well-resolved ground states are appropriately small, but the lack of clear, uncontaminated signals for certain states (namely the size 4 Polyakov loops and the 4^+) is puzzling. The 8-fold and 12-fold operators return reasonable estimates for the 0^+ and 2^+ glueballs, and the 12-fold operators produce estimates for the 4^+ and 6^+ ground states not too far from previous estimates [4]. The traditional operators return good values for the 0^+ and 2^+ spectra, and the Polyakov loop and plaquette operators display excellent agreement with accepted values. While the choice of operators used in this particular calculation appear to be too symmetric to adequately resolve the higher spin states, the utility of the superlink approach to operator construction is clearly demonstrated.

VI. CONSIDERATIONS AND IMPROVEMENTS

The use of a pre-smearing level in this context serves more to cool the lattice configuration than to control how “wide” the superlinks are, and a better approach to controlling the level of blocking in the traditional sense should be developed. Returning to the technique of removing the diagonal elements of the even powers of \mathcal{M} in Equation 11, the relative weightings of the more directional paths with unity path contributions might serve better to control how directional the superlinks are. As currently defined, these superlinks get effectively wider as their orientation approaches the diagonal: superlinks along an axis are essentially rectangular while superlinks along a pure diagonal span the full square of links in-between, see Figure 8. These exceptionally wide superlinks might explain why radial rather than angular phase cancellations seemed to dominate the higher spin operators. Retaining the unity path contributions would give more weight to the more direct paths along the diagonal. One might also consider using superlinks of length $l + 2$ rather than the minimum l used above—such superlinks would be proportionately wider and might be necessary as the lattice spacing decreases to keep the operators on a physical scale.

A direct comparison of the performance of this technique and more traditional smearing techniques has yet to be done, as well as investigating how the performance scales with dimension D and gauge group N. Such comparisons are forthcoming. The operators chosen herein seem to suffer from too much symmetry to resolve the higher spins adequately, and the negative parity and odd spin sectors need to be explored with appropriately shaped operators before the true usefulness of matrix superlinks can be determined. Relating these superlinks to those constructed previously [2, 4] by calculating the effective α of the current truncated expansion might shed light on both matrix propagator methods as well as on a new angle of approach to simulating staggered fermions on the lattice.

VII. CONCLUSION

The application of the matrix method of superlink construction has been demonstrated to agree with traditionally smeared operators and with previous methods of superlink construction. The primary difficulties with the matrix method have been alleviated by direct matrix multiplication rather than matrix inversion. The even spin, positive parity spectrum

for $\beta = 6$, $SU(2)$ in $D=2+1$ dimensions displays reasonable agreement with accepted values up to spin 6. The use of operators less symmetric than the ones presented here would resolve the odd spin and negative parity sectors. Further exploration of the matrix method of superlink construction is warranted, both to resolve the complete spin and parity spectra for $SU(N)$ in higher dimensions and to evaluate fermion determinants in $SU(N)$ with quarks.

- [1] M. J. Teper, Physical Review D **59**, 014512 (1999), URL <http://www.citebase.org/abstract?id=oai:arXiv.org:hep-lat/9804008>.
- [2] R. W. Johnson, Physical Review D **66**, 074502 (2002), URL <http://www.citebase.org/abstract?id=oai:arXiv.org:hep-lat/0206005>.
- [3] R. Johnson and M. Teper, Nuclear Physics B - Proceedings Supplements **73**, 267 (1999), URL <http://www.citebase.org/abstract?id=oai:arXiv.org:hep-lat/9808012>.
- [4] H. B. Meyer and M. J. Teper, Nuclear Physics B **658**, 113 (2003), URL <http://www.citebase.org/abstract?id=oai:arXiv.org:hep-lat/0212026>.
- [5] R. W. Johnson and M. J. Teper, Physical Review D **66**, 036006 (2002), URL <http://www.citebase.org/abstract?id=oai:arXiv.org:hep-ph/0012287>.
- [6] H. B. Meyer and M. J. Teper, Nuclear Physics B **668**, 111 (2003), URL <http://www.citebase.org/abstract?id=oai:arXiv.org:hep-lat/0306019>.
- [7] I. Montvay and G. Munster, *Quantum Fields on a Lattice* (CUP, Cambridge, England, 1994), Cambridge monographs on mathematical physics.
- [8] M. Creutz, *Quarks, Gluons, and Lattices* (CUP, Cambridge, England, 1983).
- [9] R. W. Johnson, Ph.D. thesis, Oxford University (2002), URL <http://www-astro.physics.ox.ac.uk/~rjohnson/thesis.ps>.
- [10] A. D. Kennedy and B. J. Pendleton, Physics Letters B **156**, 393 (1985).
- [11] M. Creutz, Physical Review D **36**, 515 (1987).

Plaquette Values			
$\langle U_{\square} \rangle$	$\langle U_{\square}^S \rangle$	$\langle U_{\square}^{\mathcal{M}^4} \rangle$	$\langle U_{\square}^{\widetilde{\mathcal{M}}^4} \rangle$
0.824780(1)	0.824757(2)	0.824757(2)	0.824757(2)

TABLE I: Plaquette values computed directly and with superlinks.

Polyakov Loops					
t = 1	2	3	4	5	
1.2543(1)	1.0917(2)	1.0943(4)	1.1656(14)	1.1020(80)	
1.2655(1)	1.0930(2)	1.0088(4)	1.0044(8)	0.7341(20)	
1.3143(1)	1.1085(2)	1.1085(6)	1.1957(18)	1.0795(87)	
1.3252(1)	1.1077(2)	1.0123(5)	1.0135(9)	0.7012(21)	
2.7341(1)	1.7942(11)	1.2767(48)		0	0
2.7442(2)	1.7627(13)	0.8894(52)		0	0
2.893(3)	1.9136(20)	2.3949(176)		0	0
2.9284(4)	2.3336(43)	0.7431(135)		0	0

TABLE II: Effective masses for Polyakov loops after application of the variational procedure.

0 ⁺ Box Operators				
t =	1	2	3	4
1.4356(10)	1.2316(27)	1.267(12)	1.424(043)	
1.4677(10)	1.2434(28)	1.278(13)	1.427(045)	
1.8783(15)	1.5665(67)	1.615(34)	0	
2.2646(24)	1.9433(152)	1.810(86)	0	
2.6368(29)	2.1439(255)	1.689(123)	0	
1.9374(16)	1.5797(65)	1.586(37)	0	
2.4566(28)	2.0475(220)	2.293(183)	0	
3.5028(64)	2.5556(950)	0	0	
2.9704(44)	1.9864(306)	1.633(144)	0	
3.2903(55)	1.9379(353)	0	0	
2.5172(34)	1.9597(188)	2.745(286)	0	
2.7897(36)	2.0719(265)	1.823(155)	0	

TABLE III: Effective masses for 0⁺ box operators after application of the variational procedure.

0 ⁺ Bar Operators				2 ⁺ Bar Operators			
t =	1	2	3	4	1	2	3
1.356(1)	1.202(3)	1.245(10)	1.390(34)		2.190(2)	2.060(13)	1.480(54)
1.370(1)	1.204(3)	1.251(10)	1.365(33)		2.357(2)	2.148(21)	2.315(224)
1.921(1)	1.603(8)	1.479(32)		0	2.779(4)	2.551(47)	1.060(112)
2.119(2)	1.725(12)	1.568(48)		0	2.455(2)	2.153(21)	2.069(169)
2.588(2)	2.392(3)	0		0	3.042(4)	2.619(58)	0
2.608(3)	1.773(14)	2.414(196)		0	2.631(3)	2.343(26)	0.929(84)
2.622(3)	2.360(32)	0		0	3.774(9)	3.101(222)	1.662(1.5)
3.339(6)	1.726(33)	2.553(465)		0	2.893(4)	2.280(35)	3.813(1.6)
3.783(8)	2.558(130)	0		0	2.679(3)	2.207(31)	2.075(220)
3.338(6)	2.658(83)	2.295(1.3)		0	3.711(8)	2.089(73)	0

TABLE IV: Effective masses for 0⁺ and 2⁺ bar operators after application of the variational procedure.

0 ⁺ 8-fold Operators				2 ⁺ 8-fold Operators			4 ⁺ 8-fold Operators		
t =	1	2	3	4	1	2	3	1	2
1.402(1)	1.225(3)	1.209(10)	1.187(27)		2.303(2)	1.726(11)	1.011(27)	1.894(2)	0
1.444(1)	1.229(3)	1.193(10)	1.165(27)		2.129(1)	2.098(11)	1.164(29)	2.224(2)	2.443(21)
1.857(2)	1.119(4)		0	0	2.490(2)	2.232(20)	1.806(110)	2.200(2)	2.146(15)
2.018(2)	1.404(8)	0.947(16)	1.041(51)		2.668(2)	2.453(24)	1.592(135)	2.403(2)	0
1.895(1)	1.595(8)		0	0	2.696(3)	1.793(17)	1.162(58)	2.791(3)	0
2.064(2)	1.261(6)		0	0	3.657(5)	10.80(2.1)		2.950(4)	0
2.616(3)	0.884(7)		0	0	2.629(2)	2.279(21)	1.52(78)	2.458(2)	1.694(12)
2.382(3)	1.140(8)		0	0	2.377(2)	2.163(16)	1.305(47)	3.088(5)	0

TABLE V: Effective masses for 0⁺, 2⁺, and 4⁺ 8-fold operators after application of the variational procedure.

		4 ⁺ 8-fold Overlaps								
0 ⁺		0.66	-0.277	-0.279	-0.514	-0.174	-0.221	0.231	-0.0401	
		0.622	-0.274	-0.283	-0.485	-0.167	-0.198	0.245	-0.039	
		-0.0252	0.597	0.275	0.00983	0.251	0.0596	-0.577	0.15	
		-0.381	0.00647	-0.253	0.246	0.0411	0.326	0.2	-0.0556	
		-0.466	-0.0091	0.0243	0.335	0.0235	0.15	0.0883	-0.0517	
		-0.0805	0.487	0.258	0.0487	0.194	0.0422	-0.497	0.0906	
		0.175	0.276	0.282	-0.121	0.0409	-0.107	-0.472	0.0668	
		0.291	0.219	0.238	-0.208	0.071	-0.178	-0.39	0.151	
4 ⁺		1	-0.0374	-0.242	-0.906	-0.128	-0.356	-0.0153	0.00573	
		-0.0374	1	0.176	0.0748	0.482	0.405	-0.851	0.343	
		-0.242	0.176	1	0.237	0.106	-0.506	-0.461	0.103	
		-0.906	0.0748	0.237	1	0.203	0.356	-0.0563	0.0868	
		-0.128	0.482	0.106	0.203	1	0.29	-0.554	0.873	
		-0.356	0.405	-0.506	0.356	0.29	1	-0.0964	0.159	
		-0.0153	-0.851	-0.461	-0.0563	-0.554	-0.0964	1	-0.483	
		0.00573	0.343	0.103	0.0868	0.873	0.159	-0.483	1	

TABLE VI: Timeslice overlaps for the 4⁺ 8-fold operators. Columns correspond to the various 4⁺ operators. Rows correspond to the 0⁺ and 4⁺ operators

0 ⁺ 12-fold Operators				2 ⁺ 12-fold Operators			
t =	1	2	3	4	1	2	3
1.322(1)	1.193(3)	1.207(9)	1.292(26)		2.15(1)	2.120(10)	1.638(40)
1.326(1)	1.205(3)	1.248(10)	1.464(33)		2.441(2)	2.094(15)	1.624(70)
1.695(1)	1.411(5)	1.104(14)	1.253(47)		2.384(1)	2.110(15)	1.198(42)
1.704(1)	1.439(5)	1.183(16)	1.645(78)		2.641(2)	2.104(19)	1.971(113)
2.567(3)	1.558(11)	0.966(32)		0	2.722(2)	2.643(39)	1.034(90)
2.83(4)	1.653(15)	1.345(69)		0	3.246(4)	2.873(66)	1.808(628)
2.172(2)	1.405(8)		0	0	3.720(6)	3.268(171)	0
2.541(3)	1.884(19)		0	0	2.551(2)	2.152(14)	2.825(270)
2.611(3)	1.621(15)		0	0	3.040(3)	2.701(49)	0
2.927(5)	1.413(18)	1.008(38)		0	3.525(5)	4.426(354)	0
3.065(5)	1.236(15)		0	0	2.396(2)	2.267(19)	1.186(43)
3.164(6)	1.561(28)	1.441(93)		0	2.504(2)	2.330(20)	1.324(70)

TABLE VII: Effective masses for 0⁺ and 2⁺ 12-fold operators after application of the variational procedure.

4 ⁺ 12-fold Operators		6 ⁺ 12-fold Operators		
t = 1	2	1	2	3
1.416(1)	1.235(3)	2.203(2)	2.149(18)	1.493(75)
2.044(2)	0	2.637(3)	2.384(37)	0
2.418(2)	2.953(36)	3.174(5)	0	0
3.008(4)	0	3.319(6)	2.889(117)	0
3.355(4)	0	3.479(6)	0	0
3.262(4)	0	3.749(11)	2.119(73)	0
5.924(54)	0	3.851(9)	3.094(237)	0
0	0	3.297(5)	3.639(177)	0
3.64(7)	0	3.935(10)	2.362(106)	0
0	0	3.93(11)	0	0
7.635(356)	0	3.082(4)	2.635(69)	0
3.756(7)	0	2.747(3)	2.267(36)	3.042(1.1)

TABLE VIII: Effective masses for 4⁺ and 6⁺ 12-fold operators after application of the variational procedure.

		4 ⁺ 12-fold Overlaps													
0 ⁺	0.85	-0.63	-0.48	-0.49	-0.14	0.066	-0.074	0.067	-0.02	0.11	0.079	0.092			
	-0.85	0.63	0.48	0.49	0.14	-0.066	0.074	-0.068	0.02	-0.11	-0.079	-0.092			
	-0.37	-0.049	0.39	-0.07	0.25	0.078	-0.12	0.12	-0.1	0.02	-0.066	0.069			
	0.37	0.047	-0.4	0.067	-0.26	-0.075	0.11	-0.12	0.1	-0.02	0.068	-0.068			
	-0.052	-0.18	0.14	-0.24	0.18	0.045	-0.26	0.41	0.011	0.12	-0.24	0.029			
	0.12	0.074	-0.17	0.18	-0.19	-0.024	0.28	-0.44	-0.038	-0.11	0.28	0.0039			
	0.084	-0.033	0.11	-0.16	0.22	0.0079	-0.25	0.27	0.03	0.029	-0.22	-0.05			
	0.14	-0.017	-0.29	0.27	-0.33	-0.11	0.47	-0.63	-0.026	-0.085	0.3	-0.078			
	-0.002	-0.06	0.21	-0.2	0.27	0.015	-0.29	0.35	0.026	0.045	-0.28	-0.055			
	-0.19	0.063	0.12	0.15	0.007	-0.062	0.14	-0.21	0.039	-0.034	0.024	-0.12			
4 ⁺	-0.045	0.059	-0.0092	0.27	-0.12	-0.075	0.28	-0.42	0.036	-0.097	0.12	-0.15			
	0.068	-0.085	-0.074	0.019	-0.078	-0.061	0.14	-0.18	0.038	0.023	0.034	-0.1			
	1	-0.68	-0.57	-0.59	-0.081	0.069	-0.095	0.073	-0.041	0.11	0.066	0.1			
	-0.68	1	0.21	0.81	-0.077	0.081	-0.041	-0.13	0.0064	-0.19	0.059	-0.014			
	-0.57	0.21	1	0.024	0.48	0.4	-0.38	0.15	-0.0046	-0.52	-0.036	-0.038			
	-0.59	0.81	0.024	1	-0.36	0.038	0.17	-0.46	-0.11	-0.028	0.35	0.1			
	-0.081	-0.077	0.48	-0.36	1	-0.032	-0.51	0.054	0.49	-0.069	-0.36	-0.57			
	0.069	0.081	0.4	0.038	-0.032	1	-0.58	0.24	-0.27	-0.5	0.35	0.46			
	-0.095	-0.041	-0.38	0.17	-0.51	-0.58	1	-0.4	-0.12	0.18	-0.014	-0.083			
	0.073	-0.13	0.15	-0.46	0.054	0.24	-0.4	1	-0.13	-0.075	-0.43	0.28			
4 ⁺	-0.041	0.0064	-0.0046	-0.11	0.49	-0.27	-0.12	-0.13	1	0.25	-0.044	-0.69			
	0.11	-0.19	-0.52	-0.028	-0.069	-0.5	0.18	-0.075	0.25	1	-0.13	-0.26			
	0.066	0.059	-0.036	0.35	-0.36	0.35	-0.014	-0.43	-0.044	-0.13	1	0.27			
	0.1	-0.014	-0.038	0.1	-0.57	0.46	-0.083	0.28	-0.69	-0.26	0.27	1			

TABLE IX: Timeslice overlaps for the 4⁺ 12-fold operators. Columns correspond to the various 4⁺ operators. Rows correspond to the 0⁺ and 4⁺ operators

		6 ⁺ 12-fold Overlaps											
2 ⁺	0.65	-0.19	0.099	0.05	-0.075	0.017	-0.058	0.17	-0.093	0.046	-0.31	0.43	
	-0.59	0.6	-0.22	-0.038	0.044	0.05	0.094	-0.26	0.11	-0.025	0.015	-0.57	
	-0.54	0.0029	0.038	-0.058	0.019	-0.17	-0.054	-0.035	0.027	-0.056	0.34	-0.23	
	0.52	-0.44	0.15	0.023	-0.03	-0.14	-0.19	0.28	-0.15	0.059	-0.092	0.55	
	-0.38	0.69	-0.53	-0.044	0.096	0.15	-0.01	-0.25	0.03	0.11	-0.21	-0.48	
	-0.11	0.076	-0.58	-0.18	0.32	0.078	-0.33	0.13	-0.15	0.23	0.027	0.025	
	-0.11	0.35	0.19	0.082	-0.22	0.3	0.42	-0.39	0.22	-0.2	-0.13	-0.42	
	0.16	0.27	-0.0097	0.044	-0.066	0.018	0.043	-0.04	0.005	0.016	-0.28	-0.029	
	-0.38	0.19	-0.086	-0.052	0.017	-0.081	-0.11	-0.16	0.079	-0.079	0.22	-0.27	
	0.11	-0.1	0.29	0.14	-0.1	-0.0093	0.13	-0.057	0.058	-0.048	-0.12	0.099	
	-0.63	0.32	-0.034	-0.028	0.033	-0.049	0.05	-0.15	0.11	-0.083	0.26	-0.46	
	-0.43	-0.1	0.21	-0.062	-0.012	-0.049	0.068	-0.045	0.081	-0.17	0.42	-0.23	
6 ⁺	1	-0.48	0.21	-0.029	-0.17	-0.076	-0.14	0.41	-0.2	0.041	-0.4	0.72	
	-0.48	1	-0.35	-0.15	0.0024	0.3	0.14	-0.37	0.13	-0.083	-0.35	-0.7	
	0.21	-0.35	1	-0.045	-0.16	0.022	0.28	0.02	0.24	-0.52	0.081	0.16	
	-0.029	-0.15	-0.045	1	0.28	-0.26	0.27	-0.55	0.31	0.48	0.12	0.16	
	-0.17	0.0024	-0.16	0.28	1	0.1	-0.37	-0.075	0.42	0.23	0.11	0.18	
	-0.076	0.3	0.022	-0.26	0.1	1	-0.077	-0.027	0.032	-0.17	0.05	-0.3	
	-0.14	0.14	0.28	0.27	-0.37	-0.077	1	-0.56	0.24	-0.17	0.023	-0.3	
	0.41	-0.37	0.02	-0.55	-0.075	-0.027	-0.56	1	-0.26	-0.085	-0.047	0.36	
	-0.2	0.13	0.24	0.31	0.42	0.032	0.24	-0.26	1	0.076	0.077	-0.12	
	0.041	-0.083	-0.52	0.48	0.23	-0.17	-0.17	-0.085	0.076	1	-0.0058	0.21	
	-0.4	-0.35	0.081	0.12	0.11	0.05	0.023	-0.047	0.077	-0.0058	1	-0.12	
	0.72	-0.7	0.16	0.16	0.18	-0.3	-0.3	0.36	-0.12	0.21	-0.12	1	

TABLE X: Timeslice overlaps for the 6⁺ 12-fold operators. Columns correspond to the various 6⁺ operators. Rows correspond to the 2⁺ and 6⁺ operators

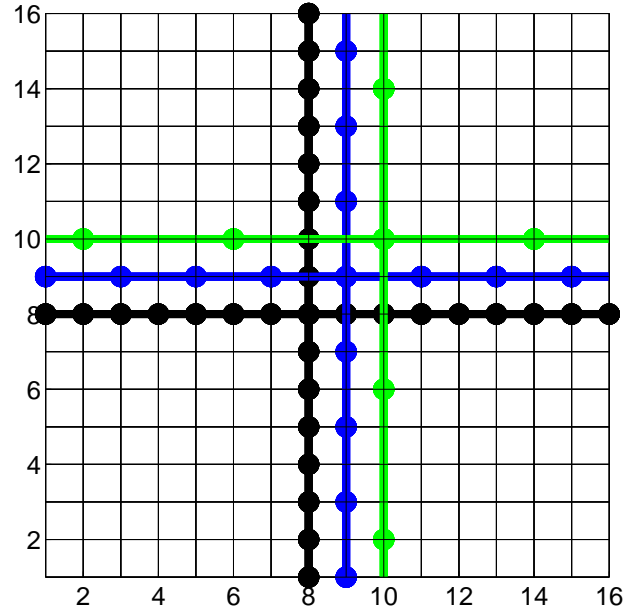


FIG. 1: Operators for Polyakov loops at sizes 1, 2, and 4.

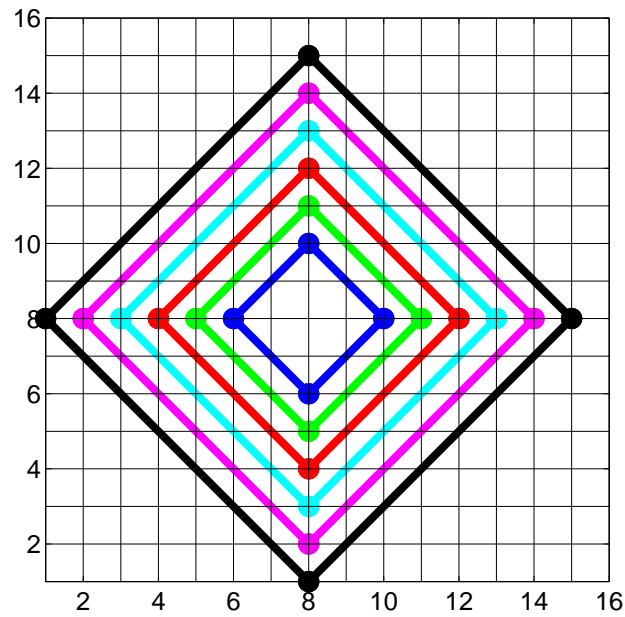


FIG. 2: Box operators at sizes 2, 3, 4, 5, 6, and 7.

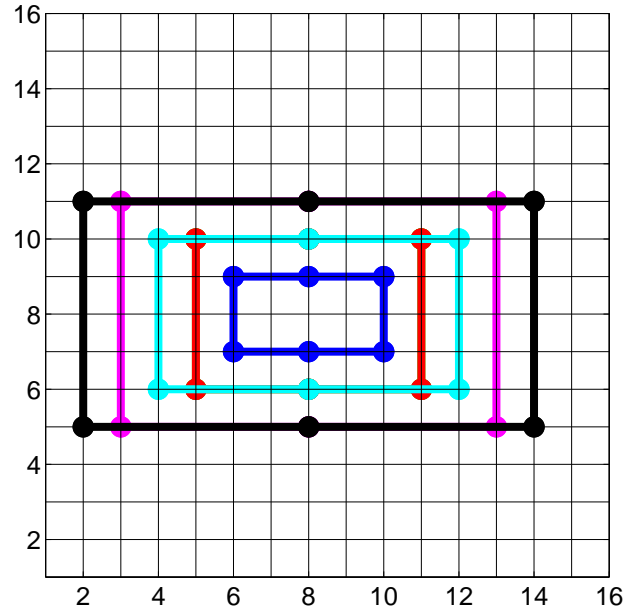


FIG. 3: Bar operators at sizes 2, 4, 5, 6, and 7.

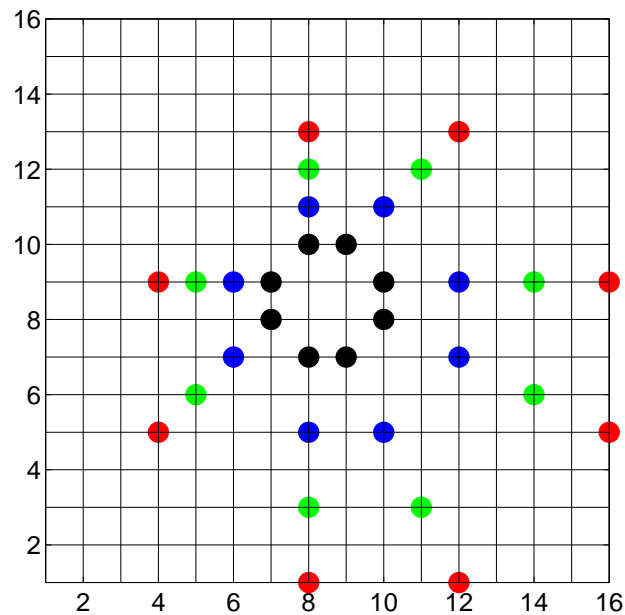


FIG. 4: 8-fold points at sizes 1, 2, 3, and 4.

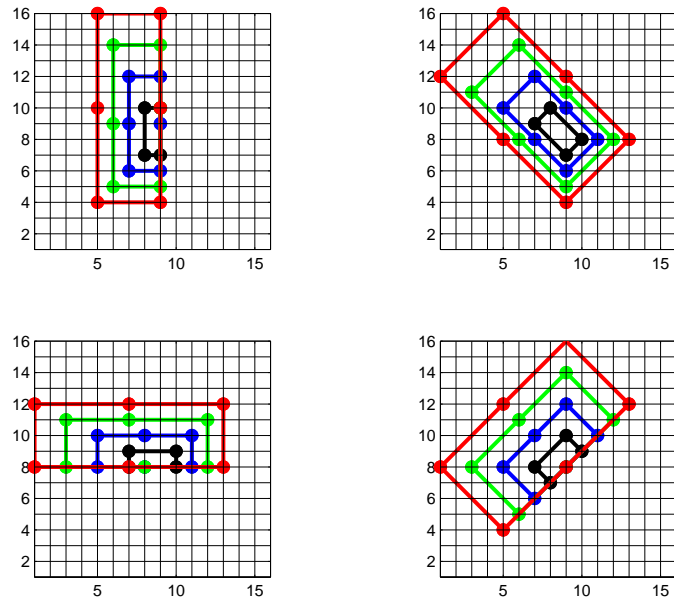


FIG. 5: 8-fold bar operators at sizes 1, 2, 3, and 4.

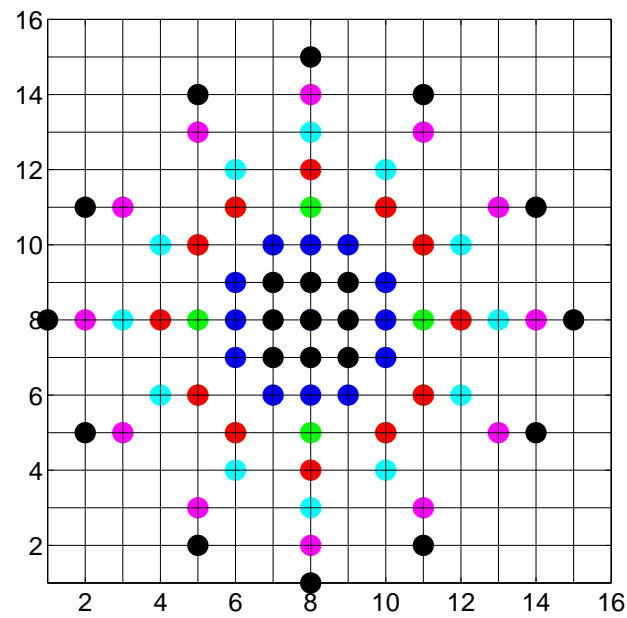


FIG. 6: 12-fold clock points at sizes 1, 2, 3, 4, 5, 6, and 7. Note the redundancy in corner points for size 1 and between sizes 3 and 4.

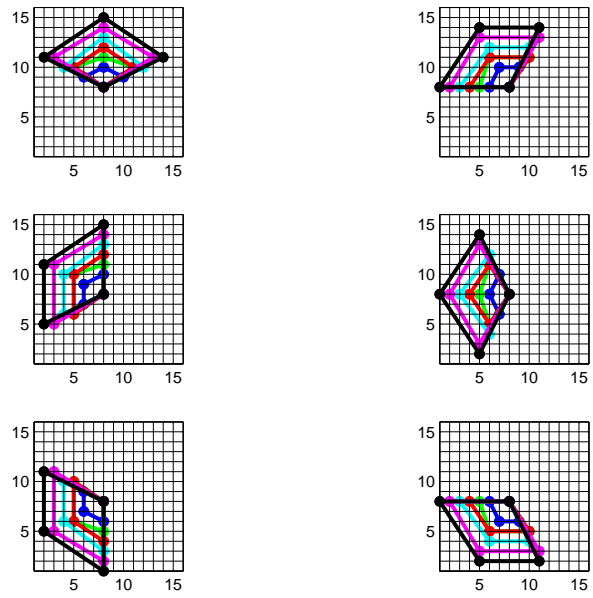


FIG. 7: 12-fold rhomboid operators at sizes 2, 3, 4, 5, 6, and 7.

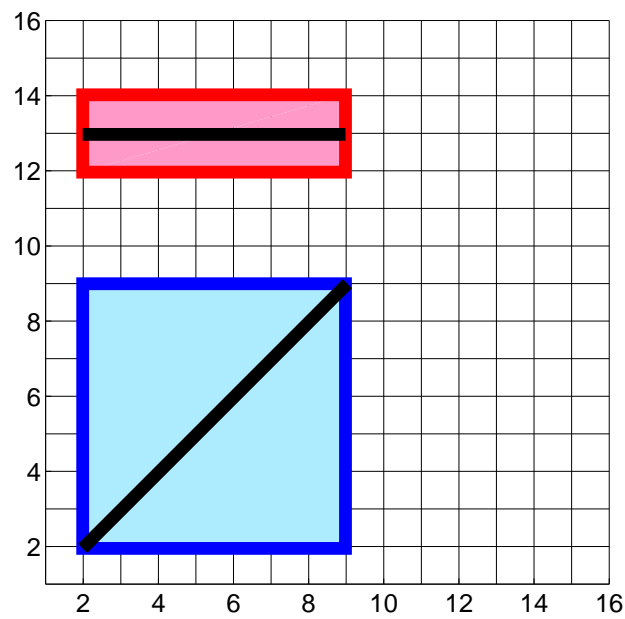


FIG. 8: Superlink widths along an axis versus along a diagonal. The superlink along the central line contains contributions from all the links covered by the surrounding shaded region.